

Revision 1, May 8, 2020

Origin, properties and structure of breyite: the second most abundant mineral
inclusion in super-deep diamonds

Word Count 5753

FRANK E. BRENNER¹, FABRIZIO NESTOLA^{2,1}, LION BRENNER¹, LUCA PERUZZO³, JEFFREY W.
HARRIS⁴

¹Geoscience Institute, Goethe University Frankfurt, Altenhoferallee 1, 60438, Frankfurt am
Main, Germany

²Dipartimento di Geoscienze, Università di Padova, Via Gradenigo, 6, 35131 Padova, Italy

³CNR-IGG, Padova, Via Gradenigo, 6, I-35131 Padova, Italy

⁴School of Geographical and Earth Sciences, University of Glasgow, G12 8QQ, Glasgow, United
Kingdom

*Corresponding Author: f.brenker@em.uni-frankfurt.de

ABSTRACT

Earth's lower mantle most likely mainly consists of ferropericlase, bridgmanite and a CaSiO₃-
phase in perovskite structure. If separately trapped in diamonds these phases can be transported
to Earth's surface without reacting with the surrounding mantle. Although all inclusions will
remain chemically pristine, only ferropericlase will stay in its original crystal structure, whereas
in almost all cases bridgmanite and CaSiO₃-perovskite will transform to their lower pressure
polymorphs. In the case of perovskite structured CaSiO₃ the new structure that is formed is
closely related to that of walstromite. This mineral is now approved by the IMA commission on
new minerals and named breyite. The crystal structure is triclinic (space group: *P*-1) with lattice
parameters $a_0 = 6.6970(4) \text{ \AA}$, $b_0 = 9.2986(7) \text{ \AA}$, $c_0 = 6.6501(4) \text{ \AA}$, $\alpha = 83.458(6)^\circ$, $\beta =$

31 76.226(6)°, $\gamma = 69.581(7)^\circ$, $V = 376.72(4) \text{ \AA}$. The major element composition found for the
32 studied breyite is $\text{Ca}_{3.01(2)}\text{Si}_{2.98(2)}\text{O}_9$. Breyite is the second most abundant mineral inclusion after
33 ferropericlase in diamonds of super-deep origin. The occurrence of breyite has been widely
34 presumed to be a strong indication of lower mantle (> 670km depth) or at least lower transition
35 zone (> 520km depth) origin of both the host diamond and the inclusion suite.

36 In this work, we demonstrate through different formation scenarios that the finding of breyite
37 alone in a diamond is not a reliable indicator of the formation depth in the transition zone or in
38 the lower mantle and that accompanying paragenetic phases such as ferropericlase together with
39 MgSiO_3 are needed.

40

41 **Keywords:** breyite, diamonds, super-deep diamonds, Earth's mantle, transition zone, lower
42 mantle, walstromite, CaSiO_3

43

44 INTRODUCTION

45 Breyite is the analogue of what is typically called “ CaSiO_3 -walstromite” in diamond
46 research due to its composition and similar crystal structure to walstromite ($\text{Ca}_2\text{BaSi}_3\text{O}_9$). In
47 nature this mineral is only found in the so-called super-deep diamonds (Joswig et al. 1999;
48 Stachel et al. 2000; Brenker et al. 2002, 2005; Stachel et al. 2005; Anzolini et al. 2016, 2018;
49 Smith et al. 2018). These are a rare category of diamonds (about 1% of the entire population,
50 Stachel and Harris 2008), which crystallize between about 300 km and even 800 km depth (Harte
51 2010) and are well distinguishable from “lithospheric diamonds”, which crystallize at shallower
52 depths between about 120 and 220 km in the mantle.

53 Breyite is considered one of most abundant minerals in super-deep diamonds, likely to be
54 second after ferropericlase, (Mg,Fe)O, and one of the most important markers to detect such
55 diamonds (i.e. ferropericlase is stable over the entire Earth's lower-upper mantle and thus cannot
56 be considered an actual depth marker). Here we report the structure, properties and origin of this
57 important mineral in diamond research and mantle petrology.

58 Breyite studied in this work was approved by the Commission on New Minerals,
59 Nomenclature and Classification of the International Mineralogical Association under the code
60 IMA 2018-062. The holotype of breyite is deposited at the Museum of Mineralogy of the
61 University of Padova under the catalogue number MMP 20371.

62 The new mineral honours the German mineralogist, petrologist and geochemist Gerhard P.
63 Brey (born 1947). He was a Professor of Mineralogy at the Institute of Geosciences, Goethe
64 University Frankfurt, Germany, from 1994 until his retirement in 2014. Brey was a pioneer in
65 experimental petrology at high pressure conditions and well known for his development of a
66 comprehensive set of thermobarometers for lherzolites and related rocks.

67

68 **RESULTS AND DISCUSSION**

69 **Occurrence and mineral association**

70 In general and apart from ferropericlase, breyite is found associated within diamonds mainly
71 with inclusions of CaTiO₃ perovskite, β-Ca₂SiO₄ larnite, titanite-structured CaSi₂O₅ (a further
72 new phase within diamonds not officially named yet) (Brenker et al. 2005; Anzolini et al. 2016)
73 and in one case with ringwoodite (the high-pressure polymorph of olivine found in the mantle
74 transition zone between 520 and 660 km depth, Pearson et al. 2014).

75 Breyite studied in this work was found within a diamond from the Sao Luiz placer deposits
76 (Juina area, Mato Grosso State, Brazil) and was intimately associated with CaTiO_3 perovskite
77 (see Fig. 1), with a composition particularly rich in Si and Al being $\text{Ca}_{0.98}\text{Ti}_{0.83}\text{Si}_{0.13}\text{Al}_{0.06}\text{O}_3$
78 (obtained on the grain in Fig. 1 by semiquantitative EDS analysis)

79

80 **Appearance and physical properties**

81 Breyite is transparent, colorless, has a vitreous lustre and is non-fluorescent. Cleavage and
82 parting were not observed. The size of the studied crystal was approximately 140 x 150 x 100
83 microns. Physical and optical properties were determined whilst the inclusion was still partially
84 in the diamond. The density, $\rho = 3.072 \text{ g/cm}^3$ was calculated on the basis of the unit-cell volume
85 obtained by X-ray diffraction. Attempts to determine Mohs hardness failed principally because
86 of the inclusion size and the size factor prevented other direct optical or physical properties from
87 being reliably determined.

88 Anzolini et al. (2016) determined the isothermal bulk modulus and thermal expansivity, of a
89 synthetic breyite by X-ray diffraction whilst at high pressures and high temperatures. The
90 pressure-volume data gave a bulk modulus value of $K_{T0} = 78.6(1.6) \text{ GPa}$ for a first-pressure
91 derivative fixed to 4, whilst the temperature-volume data fitted to a thermal pressure equation of
92 state, provided a coefficient of thermal expansivity $\alpha_0 = 2.55(9) \times 10^{-5} \text{ K}^{-1}$ at 298 K. Such
93 thermoelastic data are useful to apply elastic geobarometry for the breyite-diamond pair in order
94 to retrieve the depth of formation (see Anzolini et al. 2016, 2018). However, in this work it was
95 not possible to apply this approach even before exposing the inclusion because its spatial
96 position was already too close to the surface of the diamond host and this precludes any attempts
97 to obtain a reliable value of the depth of formation (Mazzucchelli et al. 2018).

98

99 **Composition of breyite**

100 In order to confirm the composition, the inclusion was partially exposed (see Figure 1) by
101 drilling the diamond host with an unshielded argon beam using a JEOL cross section polisher
102 enabled to work at low temperature at the Geoscience Institute, University of Frankfurt. Electron
103 backscattered images and EDS chemical semiquantitative analyses were obtained by a CamScan
104 MX3000 electron microscope equipped with a LaB₆ source and an EDAX system installed at
105 Department of Geosciences, University of Padova. Chemical analyses were performed (25 kV
106 and ~ 25 mm working distance) on small relatively flat surface areas resulting from the cross
107 section polisher and using a well characterized nearly pure diopside (in turn measured by WDS
108 in the same Department) as a reference for calibration (Pandolfo et al. 2015). As expected from
109 previous work (e.g. Bulanova et al. 2010), our EDS analyses did not show any elements other
110 than Ca and Si above the minor element level (Fig. 2 and Table 1). The empirical formula (based
111 on 9 oxygens per formula unit) is Ca_{3.01(2)}Si_{2.98(2)}O₉; the simplified formula being Ca₃Si₃O₁₂,
112 corresponding to 48.28 wt% CaO and 51.72 wt% SiO₂ (normalized to 100 %). Just for
113 comparison, Bulanova et al. (2010) on the CaSiO₃-walstromite (previous known name of breyite)
114 beyond Ca and Si reported only Fe as main impurity with FeO = 1.87 wt%. However, for our
115 breyite no counts were measured above the background in the 6.4 keV region (Fe K α), even after
116 long acquisitions.

117

118

119

120 **Crystal structure of breyite**

121 Complete intensity X-ray diffraction data were collected on the inclusion still within its diamond
122 host. Indeed, the slight exposure (Figure 1) of the inclusion made centering the mineral easier in
123 the X-ray beam. However, the extremely large size of the diamond host with respect to the
124 inclusion was the main problem to face in collecting intensity X-ray diffraction data. The X-ray
125 data were collected using a Rigaku-Oxford Diffraction Supernova goniometer equipped with an
126 X-ray micro-source assembled with a high intensity and no noise Pilatus 200K Dectris detector
127 installed at the Department of Geosciences, University of Padova. The MoK α micro-X-ray
128 source works at 50 kV and 0.8 mA, with a sample to detector distance of 68 mm. The micro
129 source ensures a brilliance at least ten times higher than conventional sealed X-ray tubes and a
130 beam spot of about 0.120 mm. Before carrying out a complete data collection, several scans were
131 performed to verify the proper crystal centering under the X-ray beam. Such a procedure
132 generates data with similar quality to that of a routine measurement on a crystal in air.
133 The size of the inclusion was 0.060×0.020×0.015 mm³ the thickness being 0.015mm estimated
134 by micro-Raman spectroscopy. A total of 9351 reflections, down to a resolution of 0.71 Å and a
135 redundancy equal to 4, were collected giving an $F^2/\text{sig}(F^2) = 13.7$. Data completeness was
136 99.8%, but the R_{int} for *P*-1 was poor (0.129) likely due to a series of non-trivial overlaps with the
137 reflections of the diamond host. Data reduction was performed using CrysAlis Pro software
138 (Rigaku-Oxford Diffraction), which corrects for the Lorentz-polarization effect and absorption.
139 Intensity data collection and crystal structure refinement (using neutral scattering curves and
140 anisotropy for all atoms) information were performed using Shelx-97 (Sheldrick 2008) starting
141 from the model by Joswig et al. (2003). A list of 15 calculated *d* spacings from the crystal
142 structure are reported in Table 2, whereas the complete dataset of the structure can be found in
143 the deposited CIF file. In terms of refinement strategy, we performed the refinement leaving free

144 to refine the occupancy factors of the three crystallographic Ca sites and not refining the
145 occupancies of Si and O atoms. Such refinement provided a structural formula of $\text{Ca}_{0.99(1)}\text{SiO}_3$,
146 which is in perfect agreement with the chemical formula obtained by the EDS measurements and
147 demonstrating that any possible impurity could be present only in traces.

148 The first crystallographic report for breyite was published as CaSiO_3 -walstromite by
149 Joswig et al. (2003). Here we report an identical crystal structure (respecting the same
150 nomenclature) to that of Joswig et al. (2003). Breyite is a ring silicate according to the Liebau
151 classification. The crystal structure is illustrated in Figure 3 viewed down the c axis. The three
152 sites for Ca are of 6, 7, and 8- coordinated polyhedra with average distances between $\langle\text{Ca-O}\rangle$ of
153 2.362, 2.534 and 2.517 Å, respectively. The three tetrahedrally coordinated distances for $(\text{Si1O})_4$,
154 $(\text{Si2O})_4$ and $(\text{Si3O})_4$ are similar having $\langle\text{Si-O}\rangle$ of 1.635, 1.637 and 1.630 Å, respectively.

155 The three Si-O-Si angles for the silicate rings are also very similar, differences being within
156 about 2.6° of each other as follows:

157
$$\text{Si1-O3-Si2} = 124.46^\circ; \text{Si2-O6-Si3} = 121.82^\circ; \text{Si3-O9-Si1} = 122.85^\circ$$

158 The three O-T-O angles show very slightly larger differences (up to 3°) and are:

159
$$\text{O3-Si2-O6} = 100.96^\circ; \text{O6-Si3-O9} = 103.99^\circ; \text{O9-Si1-O3} = 103.17^\circ$$

160 Bridging oxygen distances are also very similar being: $\text{O3-O6} = 2.589$ Å, $\text{O3-O9} = 2.610$ Å and
161 $\text{O6-O9} = 2.612$ Å.

162

163 **Micro-Raman spectroscopy**

164 Micro-Raman spectra of breyite were obtained using a ThermoScientific DXR Raman
165 microscope installed at Department of Chemistry Sciences, University of Padova. A 532 nm
166 laser caused the excitation. The laser power was 10 mW and the Raman spectrum was collected

167 for about 900 seconds. Using a 50× objective the spatial resolution was 1 μm whereas the
168 spectral resolution was about 2.5 cm⁻¹. The five main peaks, in order of decreasing intensity, are:
169 659, 980, 127, 1040 and 159 cm⁻¹. The Raman spectrum of breyite is shown in Figure 4 and also
170 shown for a comparison is the breyite published in Smith et al. (2018) whilst still within a blue
171 super-deep diamond (see their Figure 1). As the latter breyite is under a residual pressure, the
172 Raman band shift toward higher wavenumbers, but both spectra are comparable. In terms of
173 band assignment, based on previous Raman works on Ca-silicates (e.g., Richet et al. 1998), all
174 vibrational modes above 900 cm⁻¹ are represented by Si-O stretching vibrations with non-
175 bridging (peaks between 950 and 1000 cm⁻¹) and bridging oxygens (the peak at 1040 cm⁻¹); at
176 intermediate frequencies between about 430-450 and at 745 cm⁻¹ the possible vibrational modes
177 belong to the Si-O-Si stretching and bending bridging bonds; finally, the region at lower
178 frequencies between about 130 and 430 cm⁻¹ is most likely represented by the silicate network
179 along with Ca-O stretching vibrations. As breyite has quite a variable crystal size from large 200
180 μm (Anzolini et al. 2016) down to 1-2 μm (Smith et al. 2018), it is evident that micro-Raman
181 spectroscopy is perhaps the best technique to identify breyite.

182

183 **ORIGIN OF BREYITE: IMPLICATIONS FOR THE DEPTH OF FORMATION OF SUPER-DEEP**

184 **DIAMONDS**

185 Experimental studies at high pressure with a large variety of rock compositions suggest
186 that a separate Ca-Si-O phase in the Earth's mantle exists only from the deep transition zone
187 (from about 520 km depth) into the lower mantle to beyond 1000 km depth (e.g. Irifune et al.
188 1994; Irifune and Ringwood 1993; Wu et al. 2009). The stable phase of CaSiO₃ under these
189 conditions is a cubic perovskite structure with space group *Pm-3m*. The cubic polymorph

190 transforms to a tetragonal *I4/mcm* perovskite at about 12 GPa (e.g., Thomson et al. 2019).
191 However, the only natural CaSiO₃-perovskite found still preserved within a diamond does not
192 show a cubic symmetry and appears to be orthorhombic *Pbnm* like the isostructural CaTiO₃
193 (Nestola et al. 2018).

194 Whether the precursor of breyite is cubic, tetragonal or orthorhombic perovskite needs to
195 be settled by experimental petrology, which to our knowledge has not yet been completed.

196 Based on this information, regardless if the higher pressure precursor is cubic or not, the
197 widely accepted interpretation about the origin of breyite is that it was entrapped as CaSiO₃-
198 perovskite during diamond growth in the deeper transition zone or the lower mantle (e.g. Joswig
199 et al. 1999 and Stachel et al. 2005 for a general review). During uplift of the diamond host to the
200 upper mantle, the CaSiO₃ perovskite transformed to its lower pressure polymorph breyite. The
201 exact depth of this transformation is not well defined, due to residual pressures in the inclusion,
202 ambient mantle temperature and possible effects of minor and trace elements on the stability
203 field of breyite.

204 If we take into account the pressure-temperature stability field of CaSiO₃ in the pure
205 system defined experimentally (Gasparik et al. 1994; Akaogi et al. 2004, Sueda et al. 2006),
206 depths no deeper than about 270-300 km for the transformation are proposed. Anzolini et al.
207 (2019) argued that at these depths, diamond is in its elastic regime (Anzolini et al. 2019) and due
208 to its very high bulk modulus (i.e. $K_{T0} = 444$ GPa, Prencipe et al. 2014) it would be difficult for
209 diamond to accommodate the volume change necessary to transform CaSiO₃-perovskite to
210 breyite and the fully elastic paths would provide a too low pressure; indeed such volume change
211 should only be allowed if diamond would show significant fractures at the diamond-host
212 interface. However, our own TEM studies around super-deep inclusions show a high dislocation

213 density which indicates that plastic deformation indeed occurred in the diamond host. Based on
214 thermodynamic calculations and available thermoelastic data, Anzolini et al. (2016)
215 demonstrated that the CaSiO_3 -perovskite to breyite transformation would require a volume
216 change of about 28%. Such a high volume change can be accommodated by diamond only within
217 its plastic deformation regime, which might require a depth of transformation larger than 450 km
218 (i.e. about 15 GPa) (Anzolini et al. 2016).

219 A detailed chemical tomography of several Ca-Si-O inclusions in a diamond from Kankan
220 applying synchrotron XRF techniques, have shown that the Ca to Si ratio of most inclusions
221 deviates from the expected unity of both elements, if a pure CaSiO_3 -perovskite is assumed as
222 entrapped phase (Brenker et al. 2005). From experimental work it would be possible to have the
223 Ca:Si ratio less than 1, if an SiO_2 -polymorph (e.g. stishovite) is entrapped together with the
224 CaSiO_3 -perovskite. Brenker et al. (2005) have demonstrated that some of the inclusions show
225 values of the Ca:Si ratio of more than 1.6 and concluded that this would be possible only if we
226 consider the existence of a Ca-rich lithology within Earth's upper mantle in a depth range
227 enabling the coexistence of Ca_2SiO_4 -larnite either with CaSiO_3 (CaSiO_3 -perovskite or breyite) or
228 with CaSi_2O_5 -titanite. In this case, it is no longer necessary to start with the entrapment of a
229 CaSiO_3 -perovskite which would eliminate the transformation volume enigma.

230 A compositional argument against a precursor CaSiO_3 -perovskite was raised by Walter et
231 al. (2008) due to the low Mg-content measured in several breyite inclusions, which contradicts
232 experimental data and questions that a CaSiO_3 -perovskite precursor phase was ever in contact
233 with bridgmanite or majorite under deep mantle conditions.

234 Including the information given above, we summarize possible formation scenarios of
235 breyite and how to distinguish between them. Our primary subdivision will consider breyite as a

236 back transformation product from CaSiO_3 -perovskite (1), as exsolution from $\text{Ca}(\text{Si,Ti})\text{O}_3$ -
237 perovskite (2), as a direct reaction product from larnite (Ca_2SiO_4) plus titanite-structured
238 CaSi_2O_5 (3), and finally by direct precipitation from an upper mantle Si-rich fluid percolating
239 through a carbonaceous metasediment (4). Only option (1) requires the large depths indicated
240 elsewhere, whereas options (2) to (4) allows breyite to form within the asthenospheric upper
241 mantle as well.

242 **(1) Breyite is a direct back-transformation product from CaSiO_3 perovskite.** In this
243 case, we reconsider the pressure-temperature stability field of breyite within the pure CaSiO_3 -
244 system (Gasparik et al. 1994; Akaogi et al. 2004, Sueda et al. 2006). A transformation to breyite
245 would occur between 9 GPa and 13 GPa, for an mantle temperature between about 1100 (cold
246 subduction zone, extrapolated from Abers et al. 2006) and about 2000 K (plume access T of 300
247 K, Nataf 2000), respectively. However, the entrapment pressure for the CaSiO_3 -perovskite
248 precursor must be much higher depending on the chosen composition of the experimental
249 starting material. For example, using a pyrolytic composition, Zhang and Herzberg (1994) report
250 that CaSiO_3 -perovskite only appears between about 18 and 22 GPa, at temperatures between
251 1700 and 2500 K. Starting from a mid-oceanic ridge basalt (MORB) composition, Hirose and Fei
252 (2002) showed that CaSiO_3 -perovskite does not appear at pressures lower than 23 GPa at about
253 2000 K. The CaSiO_3 phase stability field does not change dramatically if endmember
254 compositions of possible deep sea sediments are used as a starting composition (Irifune et al.
255 1994). Again the first occurrence of CaSiO_3 -perovskite is at pressures corresponding to depths of
256 the lower transition zone. Thus, all experimental results on likely mantle compositions indicate
257 that the pressure-temperature stability field of CaSiO_3 -perovskite is strongly influenced by the

258 starting composition, increasing minimum formation pressures by up to 10 GPa and placing
259 formation at least in the lower part of the transition zone.

260 Reconsidering the large volume change needed to transform CaSiO_3 -perovskite to breyite
261 the scenario discussed seems unrealistic as long as diamond is within its elastic regime.
262 However, several examples exist which clearly show that this transformation has taken place,
263 which includes but is not limited to coexisting but separated inclusions of ringwoodite with
264 breyite (Pearson et al. 2014). In general, any co-genetic Mg-rich inclusion (e.g. ferropericlasite,
265 enstatite or olivine) occurring together with breyite within the same diamond suggests an
266 entrapment depth of more than 520 km. Only if pure Ca-Si-oozes or carbonatitic melts are
267 involved a deviation from this formation depth is possible (Brenker et al. 2007).

268 **(2) breyite is formed via exsolution from CaSiO_3 - CaTiO_3 -perovskite solid solution.**

269 Kubo et al. (1997) experimentally showed that at 9 GPa up to 40 mol% of CaSiO_3 can be
270 dissolved into the perovskite structure of CaTiO_3 with complete solid solution at about 12.3 GPa.
271 Thus breyite can be formed in the upper mantle as an exsolution product at pressures below 10
272 GPa (270-300 km depth) during uplift and ascent. Complex intergrowths between these two
273 phases have been found (e.g. Bulanova et al. 2010, Zedgenizov et al. 2016). In conclusion, if
274 CaTiO_3 is the main phase the depth of formation of breyite will be in the upper mantle. Based on
275 the Si-content of the full assemblage a minimum pressure can be calculated. A lower mantle or
276 deep transition zone origin is not required at the first place but cannot be excluded.

277 **(3) Breyite is a reaction product of larnite ($\beta\text{-Ca}_2\text{SiO}_4$) and titanite-structured**

278 **CaSi_2O_5 .** Based on the stability fields in the pure CaSiO_3 system (Gasparik et al. 1994; Akaogi et
279 al. 2004, Sueda et al. 2006), the finding of polyphase inclusions of breyite, larnite ($\beta\text{-Ca}_2\text{SiO}_4$)
280 and a CaSi_2O_5 -titanite phase (Brenker et al. 2005), and elastic geobarometry calculations

281 (Anzolini et al. 2016, 2018), breyite formed as a product of a retrograde reaction between larnite
282 and titanite-structured CaSi_2O_5 at pressures between 9 and 10 GPa in the upper mantle. Breyite
283 appears as a relatively minor phase trapped between the other two more abundant phases and
284 representing a reaction product of those phases, (Brenker et al. 2005). This suggests again that
285 this super-deep diamond was formed at pressures between 9 and 14 GPa in the upper mantle still
286 above transition zone depths (< 410km), breyite forming at depths not greater than 270-300 km.

287 **(4) Breyite is a reaction product of carbonate and a Si-rich component (SiO_2 or Si-**
288 **rich fluid).** Observed high Sr, Y and Zr contents in Ca-silicate phases (including breyite itself)
289 are typical of initial carbonaceous materials (e.g. Brenker et al. 2005). Thus breyite could
290 possibly form from Ca(Mg)-carbonates reacting with a Si-rich component, like SiO_2 in
291 subducted deep sea cherts, or simply as a Si-enriched fluid percolating through carbonaceous
292 rocks. The simultaneous presence of breyite and primary carbonates (Brenker et al. 2007) would
293 support this interpretation.

294 Fedoraeva et al. (2019) demonstrated that subduction of limestones and cherts on top of a
295 hydrated basaltic crust could lead to the direct in-situ precipitation of CaSiO_3 in CaCO_3 marbles
296 through the percolation of a high silica-rich hydrous fluid. The resulting assemblage of CaSiO_3 +
297 CaCO_3 is able to survive subduction down to the diamond stability field where it melts and
298 allows breyite + larnite + diamond to crystallize. This scenario would create breyite at very low
299 pressures of about 6 GPa or even less (Fedoraeva et al. 2019). The authors further suggest that
300 this might explain polyphase inclusions of breyite + larnite observed in super deep diamonds
301 (Brenker et al. 2005, Anzolini et al. 2016). However, it fails to explain the coexistence of
302 CaSi_2O_5 -titanite with these phases, which requires at least 9 GPa in order to reach the two phase
303 stability of larnite (Ca_2SiO_4) + CaSi_2O_5 -titanite.

304 A further experimentally confirmed reaction pathway is proposed by Woodland et al.
305 (2020). In their work they showed that the melting temperature of an aragonite-coesite mixture
306 under hydrous conditions will decrease down to 900°C forming a hydrous silicate melt.
307 Reduction of this melt resulted in the crystallisation of graphite in equilibrium with breyite and
308 titanite-structured CaSi_2O_5 . They determined a maximum pressure of breyite formation of about
309 8 GPa due to the reaction $\text{CaSiO}_3 + \text{SiO}_2$ to CaSi_2O_5 . Although this adds another interesting
310 option to the upper mantle formation of breyite, inclusions in super-deep diamonds often show a
311 Ca to Si ratio well above unity, which will contradict the Si-rich assemblage proposed by
312 Woodland et al. (2020) and again it fails to explain the coexistence of CaSi_2O_5 -titanite with
313 larnite.

314

315

CONCLUSION

316 Breyite can be formed throughout the whole asthenospheric mantle, the transition zone and
317 deep into the lower mantle. However, the different formation mechanisms indicate that being on
318 its own as an inclusion in diamond is not a sufficient criteria to propose an origin in the lower
319 mantle or deep transition zone (> 520 km depth). This conclusion is only valid if other inclusions
320 such as Mg-rich co-genetic inclusions (ferropericlase, low-Ni enstatite (former MgSiO_3
321 perovskite), olivine polymorphs) are present. Furthermore, the intergrowth or coexistence within
322 the same inclusions of breyite and CaTiO_3 -perovskite indicate a former single phase of
323 $\text{Ca}(\text{Si,Ti})\text{O}_3$ -perovskite which gave a lower limit of about 9 GPa or about 250 km for the depth
324 of formation (Kubo et al., 1997). In contrast, if Ca-Si-O inclusions are detected which show a
325 Ca/Si-ratio above 1, like in the case if larnite coexists with breyite in the same inclusion, a deep
326 mantle origin is highly questionable. In this case it is by far much more likely that breyite was

327 formed in a depth range above 300 km, in order to allow either a formation within the two phase
328 field of larnite plus CaSi_2O_5 or in the upper mantle by direct precipitation from a Si-rich fluid
329 percolating through a carbonaceous metasediment. Subsequent melting and infiltration into the
330 overlying reduced mantle will form the observed two phase assemblage and the diamond host
331 (Fedoraeva et al. 2019).

332 **IMPLICATIONS**

333 The work presented here is the full description of the crystal structure of breyite, the
334 second most abundant mineral found as inclusion in super-deep diamonds. Inclusions in this rare
335 type of diamonds are the only direct mineral and rock samples from the asthenospheric mantle,
336 the transition zone and even the lower mantle. The occurrence of breyite is used in numerous
337 publications as strong indicator of an origin of at least 520km depths. In this work we discuss the
338 different formation scenarios of this important mineral, which clearly show that the sole
339 occurrence of breyite is not a sufficient indicator of its formation depth. Any published work
340 about the composition and structure of the transition zone and lower mantle should be revisited
341 and proof has to be given based on further criteria for its depth of origin.

342 343 344 **ACKNOWLEDGEMENTS**

345 FB acknowledge funding of the German Science Foundation DFG (project BR 2015 / 26-1
346 and BR 2015 / 31-1). The Diamond Trading Company (a member of the De Beers Group of
347 Companies) is sincerely thanked for the donation of the studied diamonds.

348

349

350
351
352
353
354
355
356
357
358
359
360
361
362
363
364
365
366
367
368
369
370
371
372
373

REFERENCES CITED

Abers, G.A., van Keken, P.E., Kneller, E.A., Ferris, A. and Stachnik, J.C. (2006) The thermal structure of subduction zones constrained by seismic imaging: Implications for slab dehydration and wedge flow. *Earth and Planetary Science Letters* 241, 387-397.

Akaogi, M., Yano, M., Tejima, Y., Iijima, M. and H. Kojitani, H. (2004) High-pressure transitions of diopside and wollastonite: phase equilibria and thermochemistry of $\text{CaMgSi}_2\text{O}_6$, CaSiO_3 and CaSi_2O_5 - CaTiSiO_5 system. *Physics of the Earth and Planetary Interiors*, 143, 145–156.

Anzolini, C., Angel, R.J., Merlini, M., Derzsi, M., Tokár, K., Milani, S., Krebs, M.Y., Brenker, F.E., Nestola, F., and Harris, J.W. (2016) Depth of formation of CaSiO_3 -walsstromite included in super-deep diamonds. *Lithos*, 265, 138–147.

Anzolini, C., Prencipe, M., Alvaro, M., Romano, C., Vona, A., Lorenzon, S., Smith, E.M., Brenker, F.E., Nestola, F. (2018) Depth of formation of super-deep diamonds: Raman barometry of CaSiO_3 -walsstromite inclusions. *American Mineralogist*, 103, 69-74.

Anzolini, C., Nestola, F., Mazzucchelli, M.L., Alvaro, M., Nimis, P., Gianese, A., Morganti, S., Marone, F., Campione, M., Hutchison, M.T., and Harris, J.W. (2019) Depth of diamond formation obtained from single periclase inclusions. *Geology*, 47, 219-222.

Brenker, F.E., Stachel, T., and Harris, J.W. (2002) Exhumation of lower mantle inclusions in diamond: ATEM investigation of retrograde phase transitions, reactions and exsolution. *Earth and Planetary Science Letters*, 198, 1-9.

Brenker, F.E., Vincze, L., Vekemans, B., Nasdala, L., Stachel, T., Vollmer, C., Kersten, M., Somogyi, A., Adams, F., and Joswig, W. (2005) Detection of a Ca-rich lithology in the

- 374 Earth's deep (>300 km) convecting mantle. *Earth and Planetary Science Letters*, 236, 579–
375 587.
- 376 Brenker, F.E., Vollmer, C., Vincze, L., Vekemans, B., Szymanski, A., Janssens, K., Szaloki, I.,
377 Nasdala, L., Joswig, W., and Kaminsky, F. (2007) Carbonates from the lower part of
378 transition zone or even the lower mantle. *Earth and Planetary Science Letters*, 260, 1–9.
- 379 Bulanova, G.P., Smith, C.B., Blundy, J., Walter, M.J., Kohn, S.C., Gobbo, L. and Armstrong,
380 L.S. (2010) Mineral inclusions in sublithospheric diamonds from Collier 4 kimberlite pipe,
381 Juina, Brazil: subducted protoliths, carbonated melts and primary kimberlite magmatism.
382 *Contribution to Mineralogy and Petrology*, 160, 489–510.
- 383 Fedoraeva, A.S., Shatskiy, A., and Litasov, K.D. (2019) The join $\text{CaCO}_3\text{-CaSiO}_3$ at 6 GPa with
384 implication to Ca-rich lithologies trapped by kimberlitic diamonds. *High Pressure*
385 *Research*, doi: 10.1080/08957959.2019.1660325.
- 386 Gasparik, T., Wolf, K., and Smith, C.M. (1994) Experimental determination of phase relations in
387 the CaSiO_3 system from 8 to 15 GPa. *American Mineralogist*, 79, 1219–1222.
- 388 Harte, B. (2010) Diamond formation in the deep mantle: the record of mineral inclusions and
389 their distribution in relation to mantle dehydration zones. *Mineralogical Magazine* 74, 189–
390 215.
- 391 Hirose, K., and Fei, Y.W. (2002) Subsolvus and melting phase relations of basaltic composition
392 in the uppermost lower mantle. *Geochimica et Cosmochimica Acta*, 66, 2099-2108.
- 393 Irifune, T and Ringwood, A.E. (1993) Phase transformations in subducted oceanic crust and
394 buoyancy relationships at depths of 600-800 km in the mantle. *Earth and Planetary Science*
395 *Letters*, 117, 101-110.
- 396 Irifune, T., Ringwood, A.E., and Hibberson, W.O. (1994) Subduction of continental crust and

- 397 terrigenous and pelagic sediments: an experimental study. *Earth and Planetary Science*
398 *Letters* 126, 351-368.
- 399 Joswig, W., Paulus, E.F., Winkler, B., and Milman, V. (2003) The crystal structure of CaSiO₃-
400 walstromite, a special isomorph of wollastonite-II. *Zeitschrift für Kristallographie*, 218,
401 811–818.
- 402 Joswig, W., Stachel, T., Harris, J.W., Baur, W.H., and Brey, G.P. (1999) New Ca-silicate
403 inclusions in diamonds – tracers from the lower mantle. *Earth and Planetary Science*
404 *Letters*, 173, 1–6.
- 405 Kraus, W., and Nolze, G. (2000) PowderCell for Windows, version 2.4. Federal Institute for
406 Materials Research and Testing. Berlin, Germany.
- 407 Kubo, A., Suzuki, T., Akaogi, M. (1997) High pressure phase equilibria in the CaTiO₃-CaSiO₃
408 system stability of perovskite solid solutions. *Phys Chem Minerals* 24, 488–494.
- 409 Mazzucchelli, M.L., Burnley, P., Angel, R.J., Morganti, S., Domeneghetti, M.C., Nestola, F.,
410 Alvaro, M. (2018) Elastic geothermobarometry: corrections for the geometry of the host-
411 inclusion system. *Geology*, 3, 231-234.
- 412 Nataf, H.-C. (2000) Seismic imaging of mantle plumes. *Annual Review of Earth and Planetary*
413 *Sciences* 28, 391-417.
- 414 Nestola, F., Korolev, N., Kopylova, M., Rotiroti, N., Pearson, D.G., Pamato, M.G., Alvaro, M.,
415 Peruzzo, L., Gurney, J.J., Moore, A.E., Davidson, J. (2018) CaSiO₃ perovskite in diamond
416 indicates the recycling of oceanic crust into the lower mantle. *Nature*, 555, 237-241.
- 417 Pandolfo, F., Camara, F., Domeneghetti, M.C., Alvaro, M., Nestola, F., Karato, S.I., Amulele, G.
418 (2015) Volume thermal expansion along the jadeite-diopside join. *Physics and Chemistry*
419 *of Minerals*, 42, 1-14.

- 420 Pearson, D., Brenker, F., Nestola, F., McNeill, J., Nasdala, L., Hutchison, M., Matveev, S.,
421 Mather, K., Silversmit, G., and Schmitz, S. (2014) Hydrous mantle transition zone
422 indicated by ringwoodite included within diamond. *Nature*, 507, 221–224.
- 423 Prencipe, M., Bruno, M., Nestola, F., De La Pierre, M., and Nimis, P. (2014) Toward an accurate
424 ab initio estimation of compressibility and thermal expansion of diamond in the [0, 3000
425 K] temperature and [0, 30 GPa] pressures ranges, at the hybrid HF/DFT theoretical level.
426 *American Mineralogist*, 99, 1147-1154.
- 427 Richet, P., Mysen, B.O., and Ingrin, J. (1998) High-temperature X-ray diffraction and Raman
428 spectroscopy of diopside and pseudowollastonite. *Physics and Chemistry of Minerals*, 25,
429 401-414.
- 430 Sheldrick, G.M. (2008) A short history of SHELX. *Acta Crystallographica*, A64, 112-122.
- 431 Smith, E.M., Shirey, S.B., Richardson, S.H., Nestola, F., Bullocks, E.S., Wang, J.H., and Wang,
432 W.Y. (2018) Blue boron-bearing diamonds from Earth's lower mantle. *Nature*, 560, 84-87.
- 433 Stachel, T., Brey, G.P., and Harris, J.W. (2005) Inclusions in sublithospheric diamonds:
434 Glimpses of deep Earth. *Elements*, 1, 73-78.
- 435 Stachel, T., and Harris, J.W. (2008) The origin of cratonic diamonds — constraints from mineral
436 inclusions. *Ore Geology Reviews*, 34, 5–32.
- 437 Stachel, T., Harris, J.W., Brey, G.P., and Joswig, W. (2000) Kankan diamonds (Guinea) II: lower
438 mantle inclusion parageneses. *Contributions to Mineralogy and Petrology*, 140, 16–27.
- 439 Sueda, Y., Irifune, T., Yamada, A., Inoue, T., Liu, X. and Funakoshi, K.-i. (2006) The phase
440 boundary between CaSiO₃ perovskite and Ca₂SiO₄ + CaSi₂O₅ determined by in situ X-ray
441 observations. *Geophysical Research Letters*, 33, L10307, 1-4.

- 442 Thomson, A.R., Crichton, W.A., Brodholt, J.P., Wood, I.G., Siersch, N.C., Muir, J.M.R.,
443 Dobson, D.P., Hunt, S.A. (2019) Seismic velocities of CaSiO₃ perovskite can explain
444 LLSVPs in Earth's lower mantle. *Nature*, 572, 643-647.
- 445 Walter, M.J., Bulanova, G.P., Armstrong, L.S., Keshav, S., Blundy, J.D. Gudfinnsson, G., Lord,
446 O.T., Lennie, A.R., Clark, S.M. Smith, C.B. & Gobbo, L. (2008) Primary carbonatite melt
447 from deeply subducted oceanic crust. *Nature*, 454, 622-625.
- 448 Woodland, A.B., Girnis, A.V., Bulatov, V.K., Gerhard P. Brey, G.P., and Höfer, H.E. (2020)
449 Breyite inclusions in diamond: experimental evidence for possible dual origin European
450 *Journal of Mineralogy*, 32, 171–185.
- 451 Wu, Y., Fei, Y., Jin, Z., and Liu, X. (2009) The fate of subducted Upper Continental Crust: An
452 experimental study. *Earth and Planetary Science Letters* 282, 275–284.
- 453 Zedgenizov, D.A., Ragozin, A.L., Kalinina, V.V., and Kagi, H. (2016) The mineralogy of Ca-
454 rich inclusions in sublithospheric diamonds. *Geochemistry International*, 54, 890-900.
- 455 Zhang, J.Z., and Herzberg, C. (1994) Melting experiments on anhydrous peridotite KLB-1 from
456 5.0 to 22.5 GPa. *Journal of Geophysical Research-Solid Earth*, 99, 17729-17742.

457
458

459 **FIGURE CAPTIONS**

- 460 **FIGURE 1.** Electron backscattered image of breyite still kept within its diamond host (dark grey).
461 **FIGURE 2.** Representative EDS spectrum of breyite. The spectrum shows no other elements other
462 than Ca and Si.
- 463 **FIGURE 3.** Crystal structure of breyite viewed down the c axis (a and b axes are shown on the left
464 side of the Figure in red and green, respectively). All atoms are labelled and the unit

465 cell is shown in dotted line. Si1, Si2 and Si3 occupy the three semi-transparent
 466 tetrahedra coloured in yellow, blue and green, respectively.

467 FIGURE 4. Raman spectrum of

<i>Oxide wt%</i>	<i>Spot 1</i>	<i>Spot 2</i>	<i>Spot 3</i>	<i>Spot 4</i>	<i>Average</i>
SiO ₂	53.00	50.87	52.17	51.79	51.96(0.89)
CaO	47.00	49.13	47.83	48.21	48.04(0.88)
Total	100	100	100	100	100

breyite (in blue) between 120
 and 1400 cm⁻¹. At 1333 cm⁻¹ the

470 main peak of the diamond host is shown. The overlapped spectrum in red is relative to
 471 breyite by Smith et al. (2018) for a crystal still within its diamond host and under a
 472 residual pressure, which causes a Raman band shift toward higher wavenumbers.

473
 474

475 Table 1. Semiquantitative EDS analyses for breyite.

476
 477
 478
 479
 480
 481
 482
 483
 484
 485
 486
 487
 488
 489
 490
 491
 492

Table 2. Calculated X-ray powder diffraction data (in order of decreasing *d* spacing) for breyite obtained using the software PowderCell 2.4 (Kraus and Nolze 2000) based on the structural model from the CIF.

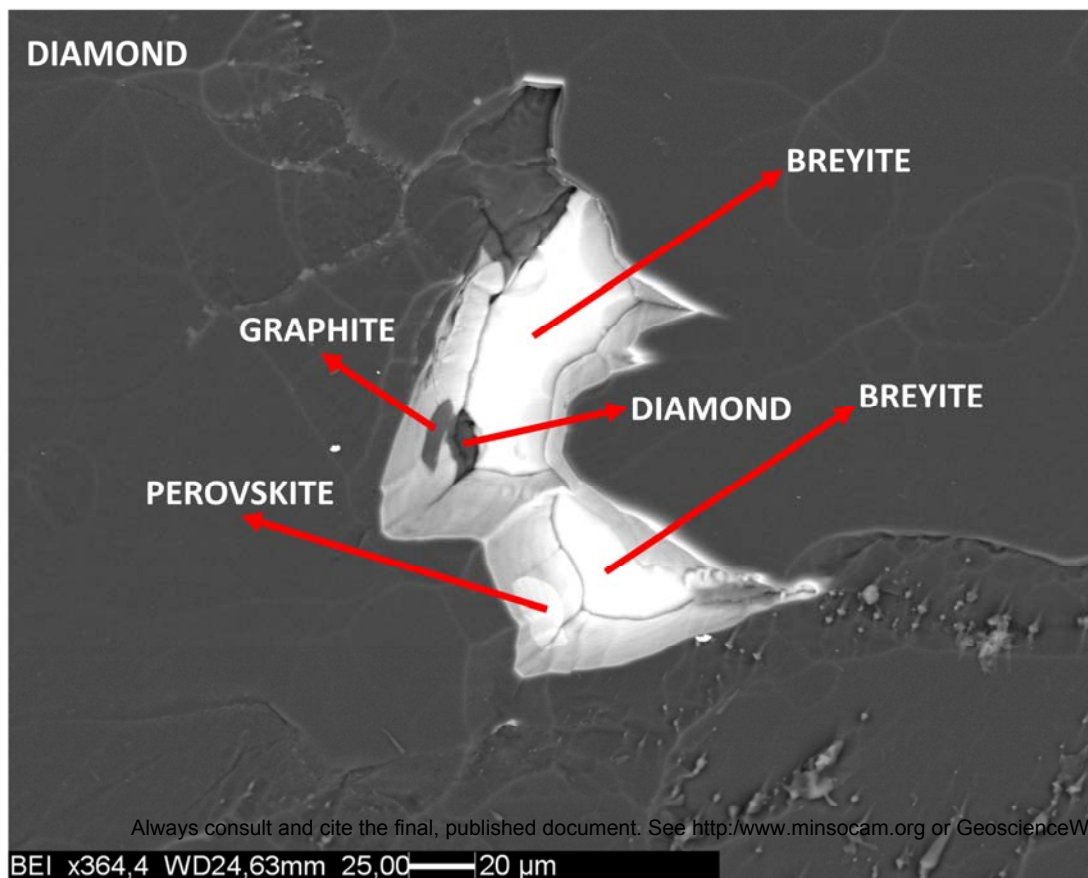
<i>h k l</i>	<i>Calculated d-spacings (Å)</i>	<i>Calculated relative intensity (%)</i>
0 1 0	8.71	12
1 0 1	5.01	32
-1 1 0	4.29	4
1 2 1	3.87	15

0 -2 1	3.55	7 493
1 1 2	3.15	40 494
2 2 0	3.03	58 495
0 3 0	2.90	100 496
-1 2 1	2.71	10 497
-2 1 0	2.63	24 498
0 -2 2	2.52	13 499
-1 -2 2	2.38	15 500
0 4 2	1.83	15 501
2 -3 1	1.79	18 502
-2 2 2	1.71	15 503

504

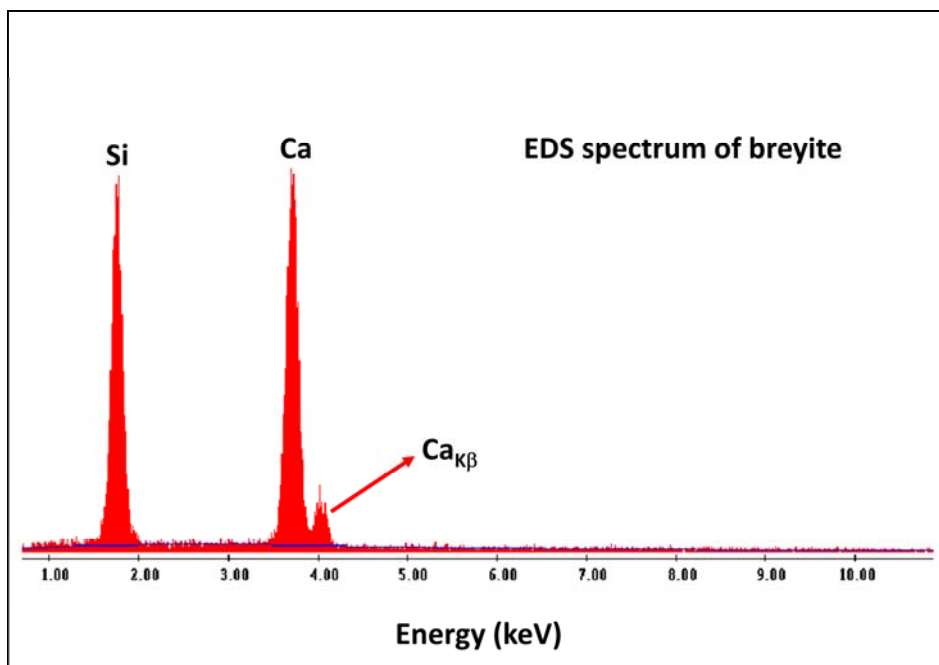
505
506
507
508
509
510
511
512
513
514
515
516
517
518
519

Figure 1



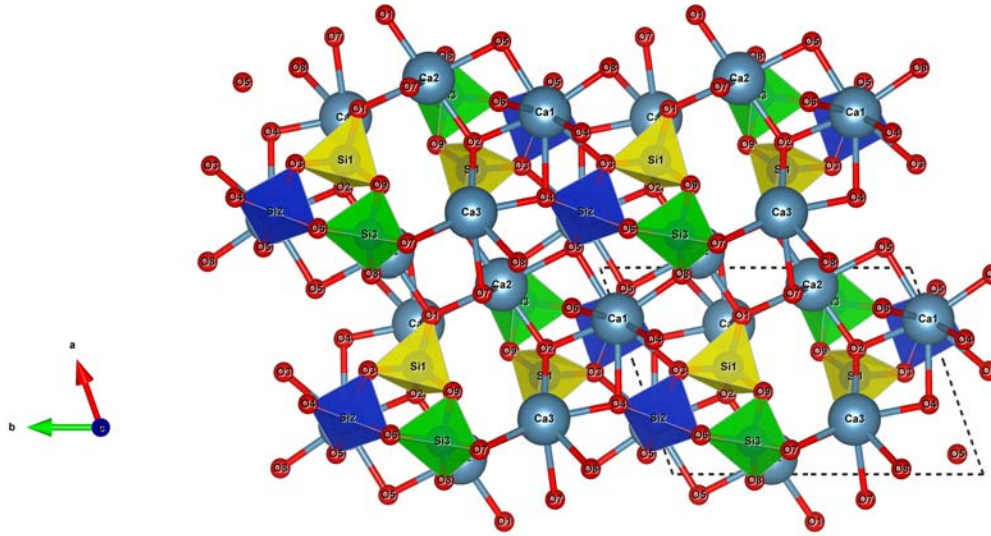
520
521
522
523
524
525
526
527
528
529
530
531
532
533
534
535
536
537
538
539
540

Figure 2



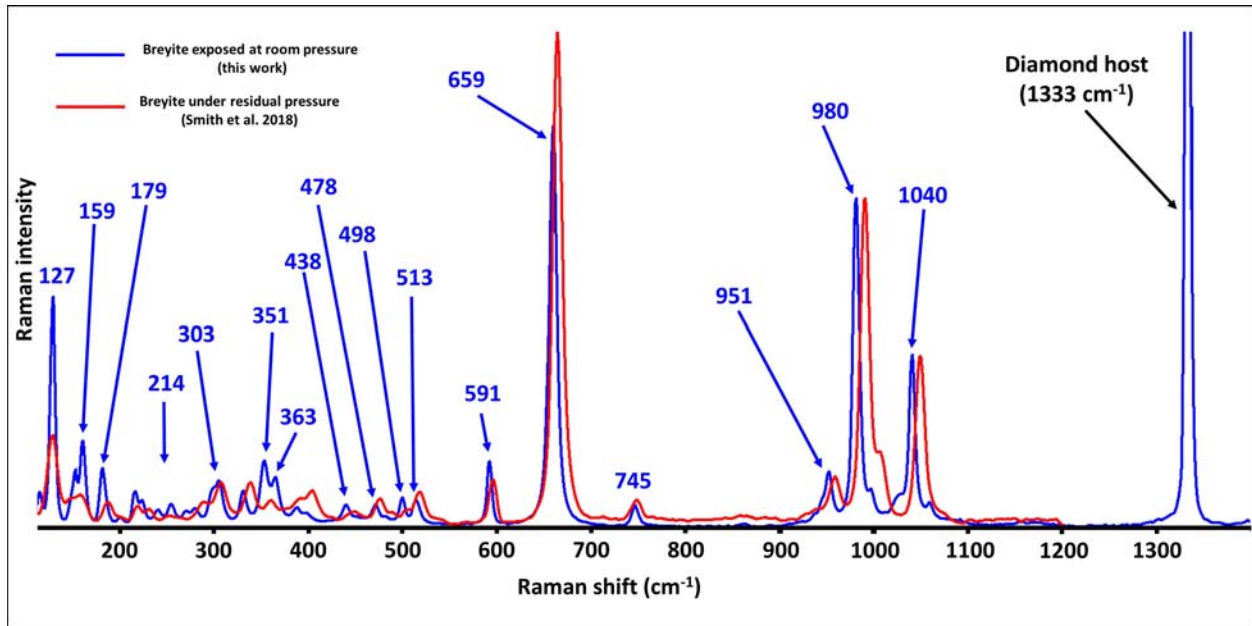
541
542
543
544

Figure 3



545
546
547
548
549
550
551

Figure 4



552
553
554
555